

# 2D Raman-THz Spectroscopy of Binary $\text{CHBr}_3$ -MeOH Solvent Mixture

A. Shalit, S. J. Mousavi, and P. Hamm\*

*Department of Chemistry, University of Zurich, Winterthurerstrasse 190,  
CH-8057 Zurich, Switzerland, peter.hamm@chem.uzh.ch*

(Dated: November 24, 2021)

**ABSTRACT:** Hybrid two-dimensional (2D) Raman-terahertz spectroscopy is used to measure the interactions between two solvents pair in the binary  $\text{CHBr}_3$ -MeOH mixture in the frequency range of 1-7 THz. Changes in the cross peak signature are monitored, originating from the coupling of an intramolecular bending mode of  $\text{CHBr}_3$  to the collective intermolecular degrees of freedom of the mixture. The appearance of a new cross peak in the 2D spectrum measured for solvent mixture with MeOH molar fraction of 0.3 indicates a coupling to a new set of low-frequency modes formed due to the hydrogen bond interactions between the two solvents. This interpretation is supported by the measurement of the  $\text{CHBr}_3$ - $\text{CS}_2$  binary solvent mixture as well as by 1D absorption measurements of neat MeOH.

## I. INTRODUCTION

Over the course of recent years, there has been significant progress in the development of time-resolved multidimensional spectroscopy techniques in the low-frequency part of the electromagnetic spectrum. Following the well-established multidimensional techniques in infrared regimes,<sup>1</sup> their low-frequency counterpart is aiming to access detailed structural information through spectral densities residing below 10 THz (1 THz = 33  $\text{cm}^{-1}$ ), where the rotational transition of molecules in the gas phase, strong transition in the semiconductor solids, and *intra/inter*molecular vibrational motion of the liquid phase can be found.

The first attempts to study the inhomogeneous nature of the low-frequency transitions in liquids were inspired by the concept of 2D Raman spectroscopy, which was proposed by Tanimura and Mukamel in 1993.<sup>2</sup> 2D Raman spectroscopy allows observing microscopic molecular dynamics through the change of the polarizability of the sample in response to the sequence of five electronically off-resonant excitations.<sup>3</sup> Despite the tremendous experimental challenges associated with the realization of the fifth-order nonlinear technique, signals from simple organic liquids such as  $\text{CS}_2$  and formamide were successfully measured.<sup>4,5</sup> Recently, a single pulse 2D Raman technique developed by Silberberg and coworkers was implemented to overcome the most significant experimental obstacle in the form of parasitic low-order cascading process<sup>6</sup> and demonstrated the ability to measure intramolecular coupling of simple halogenated liquids.<sup>7</sup> Steady progress in the generation and manipulation of strong THz fields<sup>8</sup> stimulated the development of alternative spectroscopic path toward low-frequency multidimensional spectroscopy – third-order 2D THz spectroscopy<sup>9</sup> which probes multipoint correlation function of the nuclear dipole moment of low-frequency transitions. 2D THz spectroscopy was successfully realized on molecules in a gas phase<sup>10,11</sup> and semiconductor solids<sup>12</sup>, however, the still rather limited available energies and bandwidth of THz pulses, and the experimental limitation in generation and recombination

of multiple THz pulses, have not allowed yet the realization of such experiments in liquids, where transition dipoles of the low-frequency modes are extremely small.

In an attempt to circumvent the experimental limitation of the “pure” techniques mentioned above, 2D Raman and 2D THz spectroscopy, hybrid methods, which combine indirect optical and direct THz excitation in a single experiment, were proposed and realized experimentally for various systems, including molecular liquids<sup>13–19</sup> and semiconductor solids.<sup>20</sup> Bonn and coworkers combined THz, mid-IR, and visible pulses to measure couplings between the high and low-frequency modes in liquid water.<sup>17</sup> Blake and co-workers have introduced 2D THz Raman spectroscopy with the THz-THz-Raman (TTR) pulse sequence to study halogenated liquids.<sup>14,15</sup>

At the same time in our group, an alternative hybrid method denoted 2D Raman-THz spectroscopy with the Raman-THz-THz pulse sequence (RTT) has been under steady development.<sup>13</sup> 2D Raman-THz spectroscopy allows to interrogate the low-frequency vibrational modes of liquids consecutively through impulsive (nonlinear) Raman and direct (linear) THz excitation, providing equivalent information accessible by conventional third-order echo-based spectroscopies.<sup>21,22</sup> By measuring the extent of the emitted echo signals, the approach demonstrated the ability to report on the inhomogeneity of low-frequency intermolecular modes of liquid water<sup>13</sup> and aqueous salt solutions, providing a glance into the correlation between macroscopic viscosity and structuring of hydrogen-bond networks on the molecular level.<sup>16</sup> In further work, we were able to disentangle the contribution of nuclear quantum effects to water’s structure in different water isotopologues.<sup>18</sup>

We also applied 2D Raman-THz spectroscopy to a series of halogenated organic molecules, liquid bromoform and iodoform.<sup>19</sup> This study was inspired by the work of Blake and co-workers on similar halogenated systems with THz-THz-Raman (TTR) pulse sequence mentioned earlier,<sup>14,15</sup> to see whether RTT pulse sequence can provide complementary information on these molecules. The most recent interpretation of the TTR signals by Blake

and coworkers suggested that the observed signal stems from the instantaneous excitation of intramolecular vibrations through a two-photon absorption process by a pair of strong THz fields (sum-frequency excitation pathway).<sup>23</sup> This explanation is consistent with the interpretation of the THz-Kerr effect observed earlier for similar liquids.<sup>24–27</sup> Our RTT pulse sequence lacks the strong initial THz process required for that process. Concordantly, we suggested that the RTT response originates from a different coherence pathway, initiated by a Raman induced excitation of intramolecular modes, and followed by a weak THz interaction that switches coherences from intra to intermolecular modes through two-quantum process revealing a cross peak between these two degrees of freedom.<sup>19</sup>

In this paper, we aim to test this interpretation further by measuring 2D Raman-THz spectra for a binary bromoform-methanol ( $\text{CHBr}_3$ -MeOH) solvent mixture, which is more complex with respect to its intermolecular response. To that end, we monitor changes in the cross peaks signature originating from the coupling of intramolecular symmetric bending mode of  $\text{CHBr}_3$  at  $\nu_3 = 6.7$  THz with the broad intermolecular band at about 1.5 THz as a function of the MeOH concentration in the  $\text{CHBr}_3$ -MeOH mixture.

It is well known that various excess thermodynamic properties such as the molar heat of mixing ( $H^E$ ), molar excess Gibbs free energy ( $G^E$ ), and excess volumes of mixing ( $V^E$ ) for binary solvent systems of  $n$ -alcohols with  $\text{CHCl}_3$  and  $\text{CHBr}_3$  show significant deviation from ideal behavior.<sup>28</sup> For example,  $V^E$  for the  $\text{CHBr}_3$ -MeOH solvent mixture is constantly negative throughout the entire mole fraction range,<sup>29</sup> indicating that there are specific interactions between alcohol chains and  $\text{CHBr}_3$ , which result in the volume decrease (negative  $V^E$ ). They overweight positive  $V^E$  factors such as the steric repulsion between the alcohol alkyl chains and the bulky Br atom, and the rupture of the MeOH hydrogen bond networks upon dilution with  $\text{CHBr}_3$ . It was proposed that the hydrogen bond donating ability of  $\text{CHBr}_3$  (the H atom) and the hydrogen bond accepting properties of MeOH (the O atom) are primarily responsible for the formation of networks of hydrogen bond clusters in  $\text{CHBr}_3$ -MeOH binary system. Further UV-Vis studies with various solvatochromic probe molecules in  $\text{CHCl}_3$ -MeOH mixture,<sup>30</sup> and its dynamical characterization by means of femtosecond transient absorption spectroscopy,<sup>31</sup> provided clear evidence that both molecules interact through hydrogen bond networks. Molecular dynamic simulations studies of the binary mixtures with unusual mixing behavior such as  $\text{CHCl}_3$ -MeOH and DMSO-water were carried out to quantify hydrogen-bond populations, providing insight into co-solvents interactions on the molecular level.<sup>32,33</sup> In the current study, we measure that interaction via a cross peak between a intramolecular mode of  $\text{CHBr}_3$  and the intermolecular networking modes of the binary mixture directly in the low-frequency THz spectral range.

## II. METHODS

The experimental set-up for 2D Raman-THz spectroscopy was essentially the same as described in detail before,<sup>13</sup> albeit based on a different laser system. In brief, the output of a Yb-doped fiber laser/amplifier system (short-pulse Tangerine, Amplitude Systems, France) with a central wavelength of 1030 nm, pulse duration of 150 fs, and repetition rate of 10 KHz was split into THz and Raman branches. The THz pulses were generated via optical rectification by focusing  $7 \mu\text{J}$  of the fundamental amplifier output into a  $100 \mu\text{m}$  thick (110) GaP crystal, which generated weak but broadband THz pulses with a near single-cycle shape and a bandwidth that extends to  $\sim 7$  THz (see Figure S1). The THz pulse was focused on the sample by a custom made elliptical mirror with  $2f = 83$  mm and the emitted signal was subsequently detected with an equivalent GaP crystal via electro-optic sampling with enhanced sensitivity.<sup>34</sup> Raman pulses with a central wavelength of 860 nm, bandwidth of  $\sim 9$  THz, and energy of  $5 \mu\text{J}$  were produced in an OPA (Twin STARZZ, Fastlight, France) pumped from the second harmonic of the Tangerine system.

Delay  $t_1$  between the Raman pump and the THz pulse was controlled by a step-scan motor (Physics Instruments, M-405.DG), while sampling delay  $t_2$  was scanned contentiously by a fast-scanning motor (Physics Instruments, V-408). The sample was contained in the static cuvette made of two thin sapphire windows (UQG optics) separated by a  $300 \mu\text{m}$  Teflon spacer. Data were zero-padded in both temporal dimensions, and a 2D low-pass filter with a cutoff frequency of 7 THz (determined by the available bandwidth of our spectrometer) was applied to all data. All data presented in the manuscript were collected with the same temporal window and Fourier transformed consistently.

The averaging times varied from 5 h for the pure  $\text{CHBr}_3$  sample up to a total of 80 h for the  $X_{\text{MeOH}} = 0.3$  sample. The latter was measured independently three times (see Figure S4 for the individual  $X_{\text{MeOH}} = 0.3$  measurements, evidencing the reproducibility of these results). An average over those three measurements will be shown here. Transmission of the THz field through the sample was constantly monitored during the signal acquisition to verify the molar content of the MeOH.

In contrast to our previous work,<sup>19</sup> we undersampled data along the Raman axis by a factor of 2. This reduced the signal acquisition times by the same factor, which became crucial when the much smaller signals from  $\text{CHBr}_3$ -MeOH mixtures are measured. There are two intramolecular vibrational modes (asymmetric  $\nu_6 = 4.7$  THz and symmetric  $\nu_3 = 6.7$  THz C-Br bending modes) giving rise to two cross peaks in the 2D Raman-THz spectrum due to the coupling to the intermolecular modes of  $\text{CHBr}_3$  at  $\sim 1.5$  THz.<sup>19</sup> The  $\nu_3$  mode tends to provide much stronger cross peaks signals, despite the fact that it is placed on the edge of the detection bandwidth of our 2D spectrometer. Under-sampling along the Raman axis results in

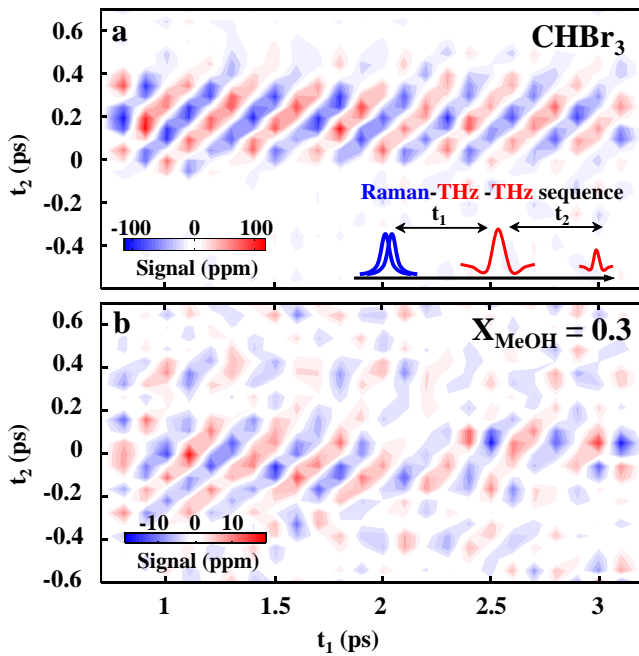


FIG. 1: Experimental 2D Raman-THz data for a) neat  $\text{CHBr}_3$  and b)  $\text{CHBr}_3$ -MeOH binary mixture with  $X_{\text{MeOH}} = 0.3$ .

the “folding” of the 6.7 THz mode into the rephasing part of the 2D spectra and inherent separation of that signal from the weak contribution of the  $\nu_6$  mode. Such an under-sampling acquisition is allowed due to inherent suppression of the rephasing part of the emitted signal by the specific spectral shape of the instrument response function (IRF) of our 2D Raman-THz spectrometer (for a detailed discussion see<sup>19</sup>). In all representations of 2D spectra, the data are folded back into the non-rephasing quadrant.

### III. RESULTS AND DISCUSSION

We start in Figures 1a and 2 with neat  $\text{CHBr}_3$ , which we have also investigated in our previous works,<sup>19</sup> but has been measured again for a consistent comparison with the subsequent dilution series. Figure 1a shows its 2D Raman-THz signal in the Raman-THz-THz quadrant measured beyond the pulse overlap region ( $t_1 > 0.7$  ps). The vibrational signal was isolated from rotational contributions, which originate from the alignment of the  $\text{CHBr}_3$  molecules along the polarization direction of the strong Raman pulse, by subtracting a single-exponential fit along each  $t_1$  cut. There is a very long-lived oscillatory signal along the  $t_1$  direction (Raman to THz delay), extending significantly beyond our measurement window, while the signal decays significantly faster along  $t_2$  axis (THz to THz delay). It appears to be a rephasing signal with the fringes inclined along the diagonal, but that is

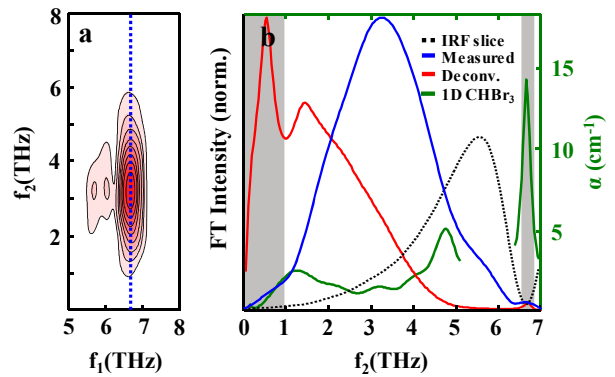


FIG. 2: a) Absolute value of the 2D Fourier transform for the neat  $\text{CHBr}_3$  signal in Figure 1a. (b) 1D vertical cut through the 2D spectrum at  $f_1 = 6.7$  THz (blue line), together with the deconvoluted data (red line) obtained by dividing through the IRF slice (black dashed line), and linear THz spectrum of neat  $\text{CHBr}_3$  (green line). The regions with unreliable deconvolution are shaded out and region contaminated by the response of the sapphire window was removed from the 1D THz absorption spectrum of  $\text{CHBr}_3$ .

an artifact from the undersampled acquisition along  $t_1$  (see **Methods**). Figure 1b depicts the signal obtained for the  $\text{CHBr}_3$ -MeOH binary solvent mixture with the highest MeOH molar fraction  $X_{\text{MeOH}} = 0.3$  used. At the same timework. Two main differences can be noticed upon MeOH dilution: a significant decrease in signal size (more than a factor of 5) and additional beating of the oscillatory signal along the THz ( $t_2$ ) axis with a nodal line around  $t_2 = 0.25$  ps. Both effects will be quantified and discussed in detail below.

Figure 2a shows the absolute value of the 2D Fourier transformation of the data in Figure 1a, revealing a single cross peak with the  $f_1$  frequency matching exactly the  $\nu_3$  symmetric bending mode of  $\text{CHBr}_3$ . Along the  $f_2$  axis, it shows a broad band peaking at around 3.3 THz, as is evident from the cut in Figure 2b, blue line. As discussed in great details in our previous publication,<sup>19</sup> the convolution of the molecular response with the IRF significantly distorts position, shape, and amplitude of the observed peaks in the 2D spectrum. In order to decipher the real frequency position of the observed cross peaks, one needs to reconstruct the IRF by taking into consideration temporal shapes of THz and Raman pulses, and subsequently perform a deconvolution by dividing the measured response through IRF in the frequency domain. In Figure 2b, the red line shows the result of that procedure, with the cross peak shifted downwards significantly along the  $f_2$  axis, now peaking at 1.5 THz. This coincides with vibrational modes, which are commonly assigned to the collective intermolecular motions of  $\text{CHBr}_3$ , and which can be seen in 1D THz absorption spectrum (Figure 2b, green line) and many other polar liquids.<sup>35,36</sup>

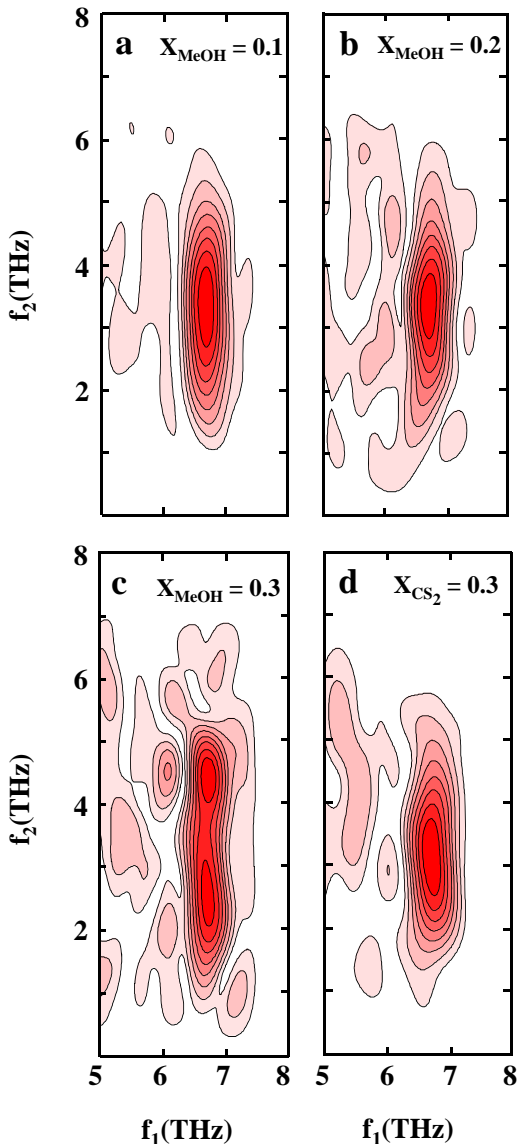


FIG. 3: Absolute value 2D spectra of a series of  $\text{CHBr}_3$ -MeOH binary mixtures with a)  $X_{\text{MeOH}} = 0.1$ , b)  $X_{\text{MeOH}} = 0.2$ , and c)  $X_{\text{MeOH}} = 0.3$  molar fractions. (d) Absolute value 2D spectrum of the control  $\text{CHBr}_3$ - $\text{CS}_2$  binary mixture with  $X_{\text{CS}_2} = 0.3$ .

Figures 3a-c show the absolute value 2D spectra obtained for a series of  $\text{CHBr}_3$ -MeOH mixtures with  $X_{\text{MeOH}} = 0.1, 0.2$ , and  $0.3$  mole fraction of MeOH. Figure 3d depicts the 2D spectrum obtained for a solution with  $0.3$  mole fraction of  $\text{CS}_2$  in  $\text{CHBr}_3$ , which was measured as a control. Comparison with the reference data of neat  $\text{CHBr}_3$  (Figure 2a) shows that the addition of MeOH with  $0.1$  and  $0.2$  mole fraction (Figures 2a and b) does not significantly affect the shape of the cross peak. The only significant difference is the reduction in signal size upon addition of MeOH. However, for the  $X_{\text{MeOH}}$

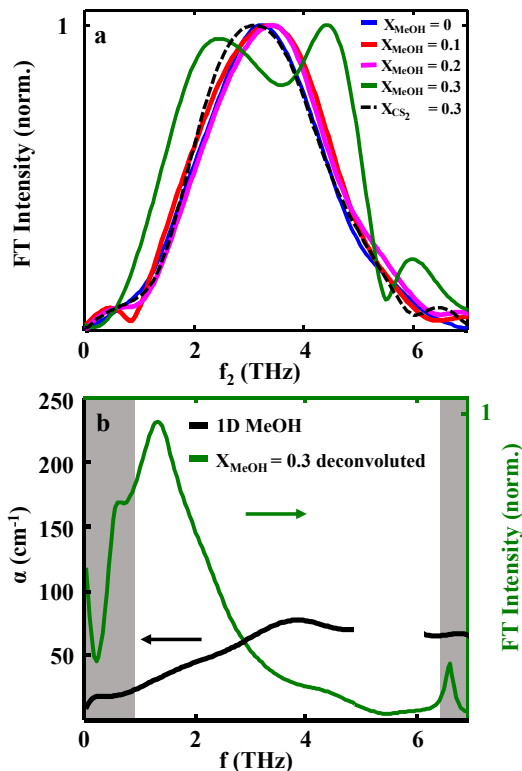


FIG. 4: a) Comparison of vertical cuts corresponding to  $f_1 = 6.7$  THz for neat  $\text{CHBr}_3$  (blue),  $X_{\text{MeOH}} = 0.1$  (red),  $X_{\text{MeOH}} = 0.2$  (magenta),  $X_{\text{MeOH}} = 0.3$  (green), and  $X_{\text{CS}_2} = 0.3$  (black dashed). b) Comparison between absorption spectrum of MeOH (black line) and deconvoluted vertical cut of  $X_{\text{MeOH}} = 0.3$  measurement at  $f_1 = 6.7$  THz. The regions with unreliable deconvolution are shaded out. The response of the sapphire windows of the cuvette was removed from 1D absorption spectrum of MeOH.

$= 0.3$  (Figure 3c), along with a further reduction of signal size, there is a significant change in the cross peak line-shape, which splits into two portions and becomes significantly broader. The origin of this split is the result of the coherent beating discussed in the context of the time-domain data of Figure 1b. On the other hand, the control measurement of a binary mixture with  $0.3$  mole fraction of  $\text{CS}_2$  does not show any significant change in the cross peak line-shape. It is important to note that we observe a quite non-trivial concentration dependence in the 2D response, while the linear absorption spectra (Figure S4) seem to be simply additive.

Figure 4a confirms that observation on a more quantitative level, depicting spectral cuts at  $f_1 = 6.7$  THz along the  $f_2$  axis for all five aforementioned measurements. The cut for the  $X_{\text{MeOH}} = 0.3$  measurement (green line) shows two peaks around  $2.4$  THz and  $4.4$  THz, while the cross peak remains in the  $3.1$ - $3.4$  THz region for the rest of the measurements, including  $X_{\text{CS}_2} = 0.3$ . As was mentioned earlier, the positions of the peaks in the 2D Raman-THz

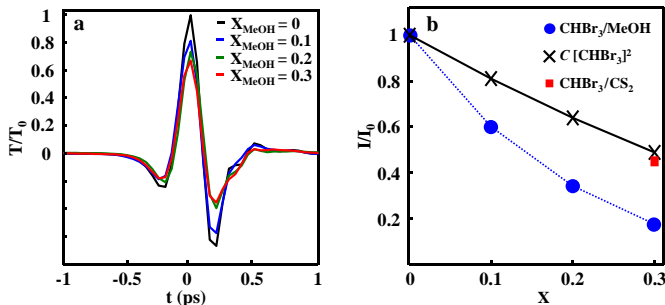


FIG. 5: a) Linear transmission of the THz field through the samples with  $X_{MeOH} = 0.1$  (blue),  $X_{MeOH} = 0.2$  (green), and  $X_{MeOH} = 0.3$  (red) normalized to the transmittance of the pure  $CHBr_3$  sample (black). b) Non-linear 2D Raman-THz size dependence on  $CHBr_3$  dilution. Measured signal vs. MeOH mole fraction (blue circles). Expected square concentration dependence (black crosses). Measured signal size for the control measurement with  $X_{CS_2} = 0.3$  (red square).

spectrum are significantly distorted and deconvolution is required to obtain the real molecular response. To get a qualitative idea about the possible origin of the splitting observed in the  $X_{MeOH} = 0.3$  sample, it is useful to analyze the spectral shape of the cross peak after deconvolution, i.e., after division by the corresponding cut of the IRF (Figure 2b, dashed black line). The result is shown in Figure 4b (green line), whose main peak is narrower and at lower frequency (1.3 THz vs 1.5 THz) as compared to neat  $CHBr_3$  (Figure 2a, red line). In addition, a small shoulder shows up around 4 THz. In order to understand the molecular origin of this shoulder, we performed a linear THz absorption measurement of a neat MeOH sample, which is depicted as black line in Figure 4b. The THz spectrum of MeOH reveals a broad peak around 3.9 THz, which was reported in the literature before<sup>37</sup> and is usually assigned, at least partially, to the collective hydrogen-bond stretching modes in MeOH.<sup>38,39</sup> The de-convoluted responses of the lower MeOH fractions and control measurements are depicted in Figure S3. While small variation in the width and position of the main peak around 1.5 THz might be interesting to investigate further, it is beyond the experimental capabilities of our 2D Raman THz spectrometer in its current state.

The fact that the frequency of the shoulder in the de-convoluted 2D Raman-THz response falls very close to the intermolecular vibration of MeOH provides evidence for the interaction between the two solvents, indicating that the intramolecular bending mode of  $CHBr_3$  is weakly coupled to the intermolecular hydrogen bond motion of MeOH. This claim can be supported further by considering the signal obtained from the control  $CHBr_3$ - $CS_2$  binary mixture (Figure 3d). Similarly to the  $CHBr_3$ -MeOH mixture,  $CHBr_3$  and  $CS_2$  are fully miscible for all mole fractions. However, unlike MeOH,  $CS_2$  lacks the

ability to form any hydrogen bond with  $CHBr_3$  and thus can be considered a simple dilution agent. Figure 3d shows that the line-shape of the cross peak remains intact upon the addition of  $CS_2$ , indicating that splitting observed in Figure 3c for  $X_{MeOH} = 0.3$  mixture is not related to  $CHBr_3$  dilution but originates from the interactions between the two solvents.

Additional indirect evidence for non-ideal behaviour is derived when examining the dependence of the signal size of the 2D response as a function of concentration of MeOH, which is significant. By the time the molar content of MeOH reaches 0.3, the non-linear 2D Raman-THz signal is decreased by a factor 5, significantly limiting our ability to measure  $CHBr_3$ -MeOH systems beyond this composition. At the same time, the linear transmittance of the THz field through  $X_{MeOH} = 0.3$  binary mixture is reduced only by  $\sim 30\%$ , as shown in Figure 5a, confirming that this sample can be still considered optically thin and no significant effects of the re-absorption are expected. This behavior is quantified in Figure 5b, where the signal size, scaled with the transmitted THz field (Figure 5a) and normalized to the maximum signal obtained for the neat  $CHBr_3$  sample (Figure 1a), is plotted against the MeOH fraction. The signal decreases much faster than the square of concentration (black line), which would be expected in the case of a simple dilution. Such a quadratic concentration dependence is expected, because cross peak signal originates from the interaction of both modes of the solvent with an intramolecular mode of bromoform. Dilution will lead to a decrease of the concentration of the  $CHBr_3$  molecules, along with a disruption of long-range interaction of the solvent, leading to a bimolecular concentration dependence. It is worth noting that when MeOH is replaced with  $CS_2$  (red square), this trivial concentration dependence is indeed observed. We believe that the “missing” signal in the  $X_{MeOH} = 0.3$  sample is an indication of the significant disruption of the long-range interaction in  $CHBr_3$  on account of the formation of new intermolecular interaction in the  $CHBr_3$ -MeOH binary solvent.

#### IV. CONCLUSION

The combination of experimental findings presented here, namely, the split of the  $\nu_3$  cross peak into two contributions in the  $X_{MeOH} = 0.3$  sample, the close correspondence of one of these cross peaks with the linear MeOH spectrum, and the non-ideal signal size dependence on MeOH concentration, provide new insights into the structure and dynamics of binary solvent mixtures. A deeper understanding of these effects will require molecular dynamics simulations, in connection with procedures to calculate the 2D-Raman THz response.<sup>40–43</sup> Such MD simulations will be demanding, since they will have to build on a polarizable and flexible force field, and since convergence of the required three-point correlation functions scales very unfavorably with the coherence time of

the system (which is long in the case of the intermolecular mode of  $\text{CHBr}_3$ ). We nevertheless hope that our work triggers effort in that direction. In any case, the double peak structure of the cross peak, or correspondingly, the beating of the time-domain data in the  $t_2$ -direction, emphasize that the response is not instantaneous in the THz dimension in our RTT pulse sequence, unlike for the TTR pulse sequence.<sup>23</sup> The demonstrated sensitivity of 2D Raman-THz spectroscopy toward low-frequency intra/intermolecular vibrational couplings can be utilized further to study structural characteristics of hydrogen bond network forming systems.

**Supporting Information:** Figure S1: Temporal and spectral profiles of the THz field generated by 100  $\mu\text{m}$  thick (110) GaP crystal. Figure S2: Absolute value 2D Raman-THz spectra obtained from three independent, non-consecutive measurements of  $X_{\text{MeOH}} = 0.3$  sample. Figure S3: Deconvoluted spectral lineshapes of the cross-peak at  $f_1 = 6.7$  THz for  $X_{\text{MeOH}} = 0.1, 0.2$ , and  $X_{\text{CS}_2} = 0.3$  mixtures. Figure S4: 1D absorption spectrum of the binary  $\text{CHBr}_3$ -MeOH mixtures.

**Acknowledgement:** The work has been supported by the Swiss National Science Foundation (SNF) through the National Center of Competence and Research (NCCR) MUST as well by the MaxWater network of the Max Planck Society.

## References:

- (1) Hamm, P.; Zanni, M. T. *Concepts and methods of 2D infrared spectroscopy*; Cambridge University Press: Cambridge, 2011.
- (2) Tanimura, Y.; Mukamel, S. Two-dimensional femtosecond vibrational spectroscopy of liquids. *J. Chem. Phys.* **1993**, *99*, 9496–9511.
- (3) Kubarych, K. J.; Milne, C. J.; Miller, R. J. D. Fifth-order two-dimensional Raman spectroscopy: a new direct probe of the liquid state. *Int. Rev. Phys. Chem.* **2003**, *22*, 497–532.
- (4) Kaufman, L. J.; Heo, J.; Ziegler, L. D.; Fleming, G. R. Heterodyne-detected fifth-order nonresonant Raman scattering from room temperature  $\text{CS}_2$ . *Phys. Rev. Lett.* **2002**, *88*, 207402.
- (5) Li, Y. L.; Huang, L.; Miller, R. J. D.; Hasegawa, T.; Tanimura, Y. Two-dimensional fifth-order Raman spectroscopy of liquid formamide: Experiment and theory. *J. Chem. Phys.* **2008**, *128*, 234507.
- (6) Frostig, H.; Bayer, T.; Dudovich, N.; Eldar, Y. C.; Silberberg, Y. Single-beam spectrally controlled two-dimensional Raman spectroscopy. *Nat. Photonics* **2015**, *9*, 339–343.
- (7) Hurwitz, I.; Raanan, D.; Ren, L.; Frostig, H.; Oulevey, P.; Bruner, B. D.; Dudovich, N.; Silberberg, Y. Single beam low frequency 2D Raman spectroscopy. *Opt. Express* **2020**, *28*, 3803–3810.
- (8) Hwang, H. Y.; Fleischer, S.; Brandt, N. C.; Jr., B. G. P.; Liu, M.; Fan, K.; Sternbach, A.; Zhang, X.; Averitt, R. D.; Nelson, K. A. A review of non-linear terahertz spectroscopy with ultrashort tabletop-laser pulses. *J. Mod. Opt.* **2015**, *62*, 1447–1479.
- (9) Elsaesser, T.; Reimann, K.; Woerner, M. *Concepts and Applications of Nonlinear Terahertz Spectroscopy*; Morgan & Claypool Publishers, 2019.
- (10) Fleischer, S.; Field, R. W.; Nelson, K. A. Commensurate Two-Quantum Coherences Induced by Time-Delayed THz Fields. *Phys. Rev. Lett.* **2012**, *109*, 123603.
- (11) Lu, J.; Zhang, Y.; Hwang, H. Y.; Ofori-Okai, B. K.; Fleischer, S.; Nelson, K. A. Nonlinear two-dimensional terahertz photon echo and rotational spectroscopy in the gas phase. *Proc. Natl. Acad. Sci. U. S. A.* **2016**, *113*, 11800–11805.
- (12) Kuehn, W.; Reimann, K.; Woerner, M.; Elsaesser, T.; Hey, R.; Schade, U. Strong Correlation of Electronic and Lattice Excitations in GaAs/AlGaAs Semiconductor Quantum Wells Revealed by Two-Dimensional Terahertz Spectroscopy. *Phys. Rev. Lett.* **2011**, *107*, 067401.
- (13) Savolainen, J.; Ahmed, S.; Hamm, P. Two-dimensional Raman-terahertz spectroscopy of water. *Proc. Natl. Acad. Sci. U. S. A.* **2013**, *110*, 20402–20407.
- (14) Finneran, I. A.; Welsch, R.; Allodi, M. A.; Miller, T. F.; Blake, G. A. Coherent two-dimensional terahertz-terahertz-Raman spectroscopy. *Proc. Natl. Acad. Sci. U. S. A.* **2016**, *113*, 6857–6861.
- (15) Finneran, I. A.; Welsch, R.; Allodi, M. A.; Miller, T. F.; Blake, G. A. 2D THz-THz-Raman Photon-Echo Spectroscopy of Molecular Vibrations in Liquid Bromoform. *J. Phys. Chem. Lett.* **2017**, *8*, 4640–4644.
- (16) Shalit, A.; Ahmed, S.; Savolainen, J.; Hamm, P. Terahertz echoes reveal the inhomogeneity of aqueous salt solutions. *Nat. Chem.* **2017**, *9*, 273–278.
- (17) Grechko, M.; Hasegawa, T.; D’Angelo, F.; Ito, H.; Turchinovich, D.; Nagata, Y.; Bonn, M. Coupling between intra- and intermolecular motions in liquid water revealed by two-dimensional terahertz-infrared-visible spectroscopy. *Nat. Commun.* **2018**, *9*, 885.
- (18) Berger, A.; Ciardi, G.; Sidler, D.; Hamm, P.; Shalit, A. Impact of nuclear quantum effects on the structural inhomogeneity of liquid water. *Proc. Natl. Acad. Sci. U. S. A.* **2019**, *116*, 2458–2463.
- (19) Ciardi, G.; Berger, A.; Hamm, P.; Shalit, A. Signatures of Intra- and Intermolecular Vibrational Coupling in Halogenated Liquids Revealed by Two-Dimensional Raman-Terahertz Spectroscopy. *J. Phys. Chem. Lett.* **2019**, *10*, 4463–4468.
- (20) Johnson, C. L.; Knighton, B. E.; Johnson, J. A. Distinguishing Nonlinear Terahertz Excitation Pathways with Two-Dimensional Spectroscopy. *Phys. Rev. Lett.* **2019**, *122*, 073901.
- (21) Hamm, P.; Savolainen, J. Two-dimensional-Raman-terahertz spectroscopy of water: Theory. *J. Chem. Phys.* **2012**, *136*, 094516.
- (22) Hamm, P.; Shalit, A. Perspective: Echoes in 2D-Raman-THz spectroscopy. *J. Chem. Phys.* **2017**, *146*, 130901.
- (23) Mead, G.; Lin, H.-W.; Magdau, I.-B.; Miller, T. F.; Blake, G. A. Sum-Frequency Signals in 2D-Terahertz-Terahertz-Raman Spectroscopy. *J. Phys. Chem. B* **2020**, *0*, Accepted.
- (24) Allodi, M. A.; Finneran, I. A.; Blake, G. A. Nonlinear terahertz coherent excitation of vibrational modes of liq-

- uids. *J. Chem. Phys.* **2015**, *143*, 234204.
- (25) Hoffmann, M. C.; Brandt, N. C.; Hwang, H. Y.; Yeh, K.-L.; Nelson, K. A. Terahertz Kerr effect. *Appl. Phys. Lett.* **2009**, *95*.
- (26) Sajadi, M.; Wolf, M.; Kampfrath, T. Transient birefringence of liquids induced by terahertz electric-field torque on permanent molecular dipoles. *Nat. Commun.* **2017**, *8*, 14963.
- (27) Kampfrath, T.; Campen, R. K.; Wolf, M.; Sajadi, M. The Nature of the Dielectric Response of Methanol Revealed by the Terahertz Kerr Effect. *J. Phys. Chem. Lett.* **2018**, *9*, 1279–1283.
- (28) Singh, P. P.; Sharma, B. R.; Sidhu, K. S. Thermodynamics of bromoform + methanol mixtures. *Aust. J. Chem.* **1978**, *31*, 1419–1423.
- (29) Singh, P. P.; Sharma, B. R.; Sidhu, K. S. Excess volumes of chloroform and bromoform mixtures with some n-alcohols at 303.15K. *Can. J. Chem.* **1978**, *56*, 2128–2127.
- (30) Gupta, S.; Rafiq, S.; Kundu, M.; Sen, P. Origin of Strong Synergism in Weakly Perturbed Binary Solvent System: A Case Study of Primary Alcohols and Chlorinated Methanes. *J. Phys. Chem. B* **2012**, *116*, 1345–1355.
- (31) Gupta, S.; Rafiq, S.; Sen, P. Dynamics of Solvent Response in Methanol–Chloroform Binary Solvent Mixture: A Case of Synergistic Solvation. *J. Phys. Chem. B* **2015**, *119*, 3135–3141.
- (32) Gratias, R.; Kessler, H. Molecular Dynamics Study on Microheterogeneity and Preferential Solvation in Methanol/Chloroform Mixtures. *J. Phys. Chem. B* **1998**, *102*, 2027–2031.
- (33) Oh, K.; Rajesh, K.; Stanton, J. F.; Baiz, C. R. Quantifying Hydrogen-Bond Populations in Dimethyl Sulfoxide/Water Mixtures. *Angew. Chem.* **2017**, *56*, 11375–11379.
- (34) Ahmed, S.; Savolainen, J.; Hamm, P. Detectivity enhancement in THz electrooptical sampling. *Rev. Sci. Instrum.* **2014**, *85*, 013114.
- (35) Davies, M.; Pardoe, G. W. F.; Chamberlain, J. E.; Gebbie, H. A. Character of absorption in far infra-red by polar molecules in liquid state. *Trans. Faraday Soc.* **1968**, *64*, 847–860.
- (36) Afsar, M.; Hasted, J.; Zafar, M.; Chamberlain, J. Absorption bands in liquid chloroform and bromoform. *Chem. Phys. Lett.* **1975**, *36*, 69 – 72.
- (37) Sarkar, S.; Saha, D.; Banerjee, S.; Mukherjee, A.; Mandal, P. Broadband terahertz dielectric spectroscopy of alcohols. *Chem. Phys. Lett.* **2017**, *678*, 65 – 71.
- (38) Garberoglio, G.; Vallauri, R. Instantaneous normal mode analysis of liquid methanol. *J. Chem. Phys.* **2001**, *115*, 395.
- (39) Woods, K. N.; Wiedemann, H. The influence of chain dynamics on the far-infrared spectrum of liquid methanol-water mixtures. *J. Chem. Phys.* **2005**, *123*, 134507.
- (40) Hasegawa, T.; Tanimura, Y. Calculating fifth-order Raman signals for various molecular liquids by equilibrium and nonequilibrium hybrid molecular dynamics simulation algorithms. *J. Chem. Phys.* **2006**, *125*, 074512.
- (41) Ito, H.; Hasegawa, T.; Tanimura, Y. Calculating two-dimensional THz-Raman-THz and Raman-THz-THz signals for various molecular liquids: The samplers. *J. Chem. Phys.* **2014**, *141*, 124503.
- (42) Hamm, P. 2D-Raman-THz spectroscopy: A sensitive test of polarizable water models. *J. Chem. Phys.* **2014**, *141*, 184201.
- (43) Magdău, I. B.; Mead, G. J.; Blake, G. A.; Miller, T. F. Interpretation of the THz-THz-Raman Spectrum of Bromoform. *J. Phys. Chem. A* **2019**, *123*, 7278–7287.

TOC Graphic:

